Editors' Suggestion

Nonlocal spin Seebeck effect in the bulk easy-plane antiferromagnet NiO

Geert R. Hoogeboom ⬤[*] and Bart J. van Wees

Physics of Nanodevices, Zernike Institute for Advanced Materials, University of Groningen,
Nijenborgh 4, 9747 AG Groningen, The Netherlands

We report the observation of magnon spin currents generated by the spin Seebeck effect (SSE) in a bulk single crystal of the easy-plane antiferromagnet NiO. A magnetic field induces a nondegeneracy and thereby an imbalance in the population of magnon modes with opposite spins. A temperature gradient then gives rise to a nonzero magnon spin current. This SSE is measured in both a local and a nonlocal geometry at 5 K in bulk NiO. The magnetic field dependence of the obtained signal is modeled by magnetic field splitting of the low-energy magnon modes, affecting the spin Seebeck coefficient. The relevant magnon modes at this temperature are linked to cubic anisotropy and magnetic dipole-dipole interactions. The nonlocal signal deviates from the expected quadratic Joule heating by saturating at a current from around 75 μA in the injector. The magnon chemical potential does not decay exponentially with distance and inhomogeneities may be the result of local magnon accumulations.

I. INTRODUCTION

Magnon spintronics is a field where spin currents are carried by magnons that exist in tunable magnets for information processing [1]. Generation of spin currents in magnets is feasible by using the spin Hall effect (SHE) in a metal injector strip creating the magnons which travel through the magnetic material to be subsequently detected at a second detecting strip [2]. Antiferromagnets (AFMs) do not possess stray fields and can therefore be exploited over a wide range of parameters such as external magnetic field and device size. Recently, this nonlocal technique has effectively been employed for the uniaxial AFMs α-Fe$_2$O$_3$ [3], MnPS$_3$ [4], and Cr$_2$O$_3$ [5]. Despite their potential for spin transport by both magnons and spin superfluidity [6], this geometry has not been employed for easy-plane antiferromagnets like NiO.

Magnons are quasiparticles carrying spin angular momentum which enables the transfer of spins in (insulating) magnets as waves of spin rotations of the magnetic moments. An easy-axis antiferromagnet has left-handed (α) and right-handed (β) magnon modes in which energies are equal but spins are opposite. Magnon interconversion is expected to equal the respective magnon chemical potentials $\mu_m^\alpha = \mu_m^\beta = \mu_m$, the deviation from the equilibrium magnon population. Magnon injection then creates a finite μ_m which drives the transport of magnon spins, following the regular discussion for magnon transport [7]. This description is equivalent to that in Refs. [8,9], where μ_α and μ_β are regarded as equal but opposite in sign because they result in opposite spin currents. Magnon spins can be injected at the interface with a paramagnetic heavy metal using the SHE or in the bulk magnet.

In the first method, α (β) magnons are created (annihilated) if the accumulated spin direction at the interface is parallel to

an α-magnon spin resulting in an increase (decrease) in the magnon chemical potential μ_m. In the latter method, heating by the injector sets up a thermal magnon current of both modes, which diffuses from the hot region to the cold region, the spin Seebeck effect (SSE). In a ferromagnet (FM) this leads to finite spin currents even without an applied magnetic field since there is one kind of magnon whose polarity is determined solely by the magnetization. In AFMs, however, there is no inherent population imbalance between the modes when they are degenerate. These modes carry equal but opposite pin currents and no net spin current arises due to a thermal gradient, so there is no spin SSE in the absence of a magnetic field. The degeneracy of these magnon modes is lifted by a magnetic field, creating an imbalance in their population and thereby net magnon spin currents can be created [10,11].

The different modes are coupled via inelastic magnon-magnon scattering, allowing for energy interchange between different modes and magnon relaxation. This results in a slight suppression of the spin Seebeck coefficient but will largely leave the transport and its magnon conductivities of both magnon modes intact [12]. The magnon depletion is expected to decay exponentially with distance in bulk magnets [12,13]. Accumulation of magnons at interfaces can be observed as a sign change in μ_m [13].

In this article, the nonlocal observation of the spin Seebeck effect in an easy-plane AFM shows that there is an imbalance between populations of the magnon modes with opposite spins. This results in a net spin current driven by the temperature gradient. The transport of magnons does not require such an imbalance. However, no electrically injected magnon spin currents, which rely on a significant spin transmission by an exchange interaction between the Pt and the NiO, have been observed. The SSE-generated spin currents have been generated at 5 K in bulk NiO containing multiple domains. There is no need of arranging the magnetic domains by the

_____
[*]g.r.hoogeboom@gmail.com

exchange interaction with a FM layer, in contrast to Ref. [14] where a FM seed layer is required to obtain a SSE signal from a 200-nm-thick NiO layer. The SSE amplitude as a function of the magnetic field strength is modeled by magnon mode splitting, creating the imbalance in the magnon population of the modes. The magnon chemical potential shows some local variation and shows an increase in noise by increasing the distance from the injector.

II. THEORY

A. Magnon modes

Easy-axis antiferromagnets have magnon modes that are typically in the terahertz regime. Easy-plane AFMs, however, have a more complex magnon dispersion, which is extended to lower energies. When considering only the exchange and anisotropy, a gap appears between the two modes [14]. Although NiO has a simple rock salt structure, magnetic dipole-dipole interactions and cubic anisotropy can give rise to multiple low-energetic precession modes, the dispersions of which depend on the magnetic field [15]. At low temperatures (a few Kelvins), the gap from Zeeman splitting is of the order of the thermal energy and therefore could induce a nonzero spin Seebeck coefficient.

A magnetic field influences the spin current via the dispersion consisting of multiple modes with different magnon spin polarizations. Reference [16] treats the dispersion of the α and β modes having an offset at the zero q point even without an applied magnetic field. The offset is said to arise from the hard-axis anisotropy and is further influenced by the Zeeman interaction when applying a magnetic field. The dispersion is then given by

$$
\begin{aligned}
\omega_{\alpha,\beta}^2/\gamma_k^2 = & \left(H_e + H_{ep} + \frac{H_{ha}}{2}\right)^2 - \frac{1}{4}H_{ha}^2 + H^2 - H_e^2\gamma_k^2 \\
& \pm \left\{ H_e^2 H_{ha}^2 \gamma_k^2 + 4H^2\left[\left(H_e + H_{ep} + \frac{H_{ha}}{2}\right)^2 \right.\right. \\
& \left.\left. - H_e^2\gamma_k^2 \right]\right\}^{\frac{1}{2}},
\end{aligned}
\tag{1}
$$

where $\gamma_k = \cos(\frac{1}{2}ka_l)$, $H_e = 968.4$ T, $H_{ha} = 635$ mT, and $H_{ep} = 11$ mT are the structure factor, the exchange interaction, and the hard-axis and easy-plane anisotropy, respectively [16–19]. The offset causes an unequal population of these modes, especially at temperatures lower than the offset temperature of the α mode. Since their magnon spin directions are considered opposite [10], this results in a net magnon spin required for a nonzero SSE. Figure 1(b) shows that the offset in the dispersions as a function of magnetic field further increases, enlarging the net magnon spin.

However, when additionally considering the symmetry breaking magnetic dipole-dipole interactions and the cubic anisotropy as done by Milano and Grimsditch [15], multiple low-energy modes appear which are shown in Fig. 1(c) for different domains and the respective magnetic moment directions as a function of the magnetic field strength. Energetically higher modes are not considered since the measurements are performed at 5 K. Under the influence of a magnetic field
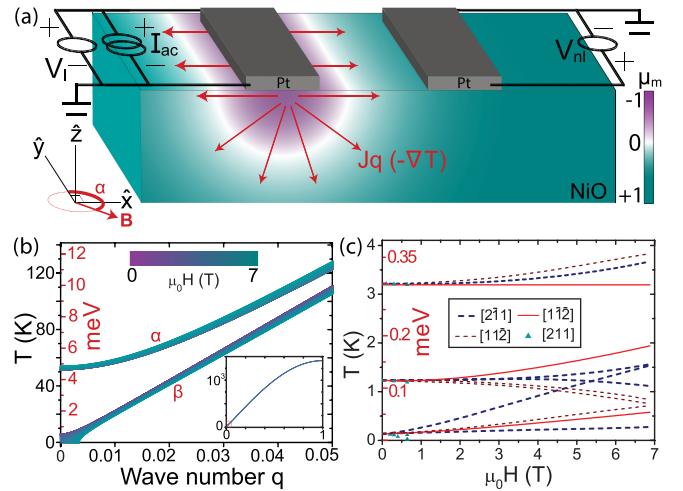

FIG. 1. (a) Device structure and probes on the NiO bulk crystal with the spin injector (left Pt strip) and detector (right Pt strip) at distances d apart, ranging from 250 nm to 7 μm. An in-plane magnetic field **B** is applied with a clockwise angle α with the y axis. A 100-μA current is sent through the injector leading to Joule heating and a radial heat gradient J_q indicated by the red arrows. A surplus of magnons on the hot side flow to the cold side, leaving behind a negative μ_m. At interfaces, magnons accumulate and can contribute to μ_m as observed in thin films of yttrium iron garnet (YIG) on gadolinium gallium garnet (GGG), the distribution of which is reproduced here [13]. μ_m is normalized in the scale. A finite μ_m results in spin transport between the Pt and the NiO via the spin mixing conductance. The inverse spin Hall effect consequently causes a voltage locally, V_l, and nonlocally, V_{nl}. (b) The magnon dispersion [Eq. (1)] after Ref. [16] of two modes as a function of a magnetic field along the easy plane considering exchange and Zeeman interaction. The inset shows the full range of the wave number q. (c) Magnon energy at the $q = 0$ point after Ref. [15] as a function of a magnetic field along [110] when taking magnetic dipole-dipole interactions and cubic anisotropy into account. This breaks the symmetry and splits the magnon energies with [2$\bar{1}$1] spin directions. The energies are given in Kelvin (black) and meV (red).

within a $\langle 111 \rangle$ easy plane (along [110]), the [2$\bar{1}$1] magnon modes and to a lesser extend the [11$\bar{2}$] magnon modes split, the [11$\bar{2}$] magnon modes remain degenerate, while the [211] modes are soft and become unstable from 0.55 T. A magnetic field thus causes an inbalance in the occupation of these modes which have different magnon spin direction. This leads to an imbalance in the magnon populations and opens up the opportunity to investigate these magnons with the SSE.

B. Spin seebeck effect

When there is a net magnon spin population in a magnetic material, a temperature gradient can drive a magnon spin current $J_s = -(\sigma_m \nabla \mu_m + S \nabla T)$ via the SSE. The spin Seebeck coefficient S has a field and a temperature dependence. The flow of magnons creates a negative magnon chemical potential μ_m near the injector. Boundary conditions at interfaces [13], and, possibly, domain walls and defects, lead to magnon accumulation and reflection resulting in a positive sign of μ_m at a distance from the injector. Shown in Fig. 1(a) is the distribution of μ_m as a result of such reflections at the interface

of a thin film of YIG on GGG. A spin current enters a Pt strip via a finite spin mixing conductance where it is converted to a charge current by the inverse spin Hall effect.

A SSE generated spin current has been observed from NiO when grown on a FM to force the preference of one type of the many possible domains by the exchange interaction which is stronger with an uncompensated ferromagnetic ⟨111⟩ layer. These domains are said to have an anisotropy-induced splitting without a magnetic field and having only one type of domain would result in a nonzero SSE [14]. Without the seed layer of Py below the grown NiO, no SSE was observed as the spin currents originating from different domains would cancel [14]. Signals in such systems show hysteresis and decrease in size when decreasing the temperature, vanishing below 100 K [20].

C. Spin Hall magnetoresistance

The spin Hall magnetoresistance (SMR) is the first harmonic response and can be obtained simultaneously with the second harmonic SSE with a lock-in technique [21]. The SMR of the Pt injector strip is sensitive to the magnetic moments underneath it, even to the Néel vector in antiferromagnets [22]. The SHE deflects electrons in a direction depending on their electron spin, resulting in the accumulation of electron spins at the interface with NiO. The direction of these electron spins is affected by the interaction with the magnetic moments in the NiO via the spin transfer torque. This exchange interaction is maximal when the directions of the magnetic moments and the accumulated electron spin are perpendicular. The electron spin is reflected back into the Pt and subsequently deflected by the inverse spin Hall effect determined by the electron spin. Absorption of the spin by the magnet thereby affects the path traveled by the electrons and influences the longitudinal resistivity ρ_L of the Pt layer by [22,23]

$$\rho_L = \rho + \Delta\rho_0 + \Delta\rho_1\left(1 - n_x^2\right), \tag{2}$$

where $\langle n_x \rangle$ is the average of the Néel vector along $\hat{x}$ just below the Pt injector. This technique thus indicates the influence of the magnetic field on the magnetic moments; i.e., it gives information about the magnetic order and domain wall growth.

D. Properties of NiO

NiO is a cubic material with antiferromagnetic interaction due to superexchange between two Ni atoms via an oxygen ion. Together with magnetic dipole-dipole interactions and a small cubic anisotropy this results in the spins aligning in ferromagnetic {111} planes which are intercoupled antiferromagnetically [24]. The magnetic moments themselves align along [11$\bar{2}$] within these {111} planes, although a minor diversion can be induced by anisotropy [24] or rhombohedral distortion. Due to magnetostriction the crystal is rhombohedrally distorted along the ⟨111⟩ directions and magnetic twin (T) domains are formed [25]. Within a T domain, the three easy axes give rise to corresponding spin rotation (S) domains. By introducing a magnetic field, the degeneracy of energetically equivalent domains is lifted, resulting in a redistribution of these domains by movement of the do-
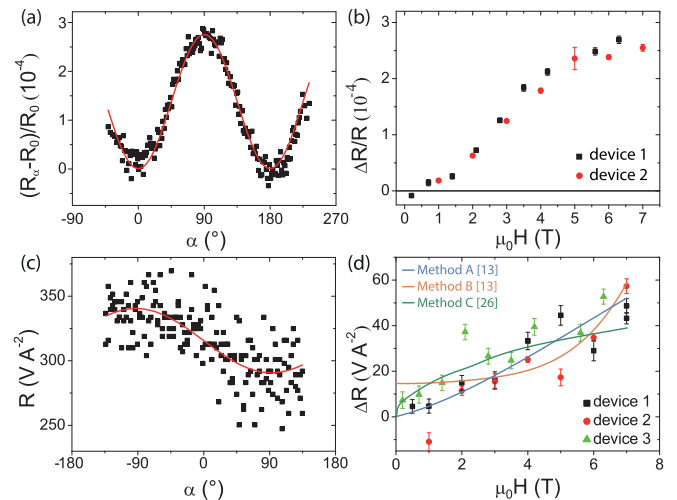

FIG. 2. (a) Spin Hall magnetoresistance as a function of the in-plane rotation angle α, performed at 6.3 T and 5 K. R_α is the angle-dependent resistance of the Pt strip and R_0 is the base resistance of 5.17 kω. (b) Amplitude of the SMR signals as a function of the magnetic field strength, showing a similar curve as reported in [22] for both devices. (c) The locally observed signal changes from the spin Seebeck effect as a function of the magnetic field angle at 6.3 T. (d) The amplitude of the signal increases monotoneously with field with little offset, modelled by the three methods described in the main text. The error bars in panels (b) and (d) represent the fit uncertainty.

main walls. The direct influence on the spin rotation causes movement of the S domains. Domain walls can influence the rotation of the Néel vector and thereby both the SMR and the SSE.

III. METHOD

The bulk NiO sample was commercially obtained and polished along a ⟨111⟩ plane as described in Ref. [22]. Thereafter, the devices were fabricated using electron beam lithography. No etching was performed before the sputtering of the 5-nm-thick, 20-μm-long, and 100-nm-wide Pt strips. Three devices were fabricated with distances between the Pt strips of 250 nm to 7 μm.

IV. RESULTS AND DISCUSSION

The SMR measurements show a $\sin^2 \alpha$ angle dependence [see Fig. 2(a)]. The changes in the magnetic moments are such that they tend to align perpendicular to the magnetic field direction, so as to maximize the negative Zeeman energy. The signals are therefore 90° angular shifted as compared to Pt|FM systems, confirming antiferromagnetic order in the material [22]. Similar to our earlier work on this sample [22], the amplitudes of such rotation measurements initially increase quadratically as a function of the field strength and a saturation sets in which is established around 6 T [see Fig. 2(b)]. This field dependence is believed to be originating from both anisotropy and domain wall movement. As domains with the magnetic easy plane in the ⟨111⟩ surface plane become more favored over other domains, these domains grow in size [22,26]. The domain size at small field must be smaller

than the Pt strip's size to follow the same field dependence as a Hall bar device. This agrees well with the observed domain size of $< 1 \mu$m [27]. A domain wall can affect magnon spin currents and therefore the distribution of magnon chemical potential as well. At saturated field strengths, the magnetic moments are coherently rotated by the magnetic field and the crystal is more or less in a single magnetic domain.

The locally measured current-induced SSE shows an angular dependence and signal size which are similar to those of local measurements of Pt on FMs [see Fig. 2(c)]. The noise of 40 V A^{-2} is relatively large in comparison to Pt|FM systems and might be originating from domain walls that move due to the changing magnetic field direction. There is a background signal of which the origin can be other heat-related effects such as the spin Nernst or the Righi-Leduc effect. The size of the signal amplitude as a function of the magnetic field strength shows on average a monotonous increase for all three devices as shown in Fig. 2(d) apart from the substantial variation between measurements.

The SSE amplitude as a function of the magnetic field strength was fitted using the contribution of the different modes by methods A and B described in Ref. [16] and method C from Ref. [28]. The magnon dispersion from Eq. (1) has been used in method B and the zero q-point value has been altered by the data of Ref. [15] presented in Fig. 1(c) for methods A and C, assuming that only small q values play a role at the low temperature of 5 K. It is assumed that the magnons are close to the thermodynamic equilibrium, allowing the use the Bose-Einstein distribution for both magnon branches at a temperature of the phonon bath [12,16]. For methods A and B, the spin Seebeck coefficient of the splitted magnon modes is given by

$$S_S^z = S_0 \int dk k^2 \left[\frac{e^{\frac{\hbar \omega_{\beta k}}{k_B T}} \omega_{\beta k} v_{\beta k y}^2}{\eta_{\beta k} \left(e^{\frac{\hbar \omega_{\beta k}}{k_B T}} - 1 \right)^2} - \frac{e^{\frac{\hbar \omega_{\alpha k}}{k_B T}} \omega_{\alpha k} v_{\alpha k y}^2}{\eta_{\alpha k} \left(e^{\frac{\hbar \omega_{\alpha k}}{k_B T}} - 1 \right)^2} \right], \quad (3)$$

where $S_0 = \frac{\hbar}{6\pi^2 k_B T^2}$, $\omega_{\mu k}$ is the field-dependent frequency, and $\eta_{\mu k}$ is the magnon relaxation rate of the magnon mode μ as function of the wave vector k. Further we need the magnon group velocity $v_{\mu k} = \delta \omega_{\mu k}/\delta k$ and the relaxation rate $\eta_q = 1 + (1240q + 5860q^3)(T/300)^3$ [28]. The values are numerically solved at a large set of field strengths whose interpolating function can be fitted to the SSE amplitude data as a function of the field strength. Using the method described in Ref. [16] this amounts to $S_S^z = 7.8 \times 10^{-11}$ erg cm^{-1} K^{-1} for the dispersion in Eq. (1) (method A) and $S_S^z = 2.4 \times 10^{-11}$ erg cm^{-1} K^{-1} using the adjusted dispersion (method B) at 7 T.

Both the near linear increase and the relatively small offset in the data are not represented by method B, which instead shows a large offset and an approximately quadratic increase with field strength. Possibly these modes disappear due to spin reorientations when applying a field. By following the model described in Ref. [16] and using Eq. (1), the field dependence shows saturating behavior and a less significant offset. When using the dispersion including the effects of magnetic dipole-dipole interactions and cubic anisotropy, the SSE field dependence resembles the data and no offset is present. At 20 K the signal has reduced to $(3.2 \pm 0.3) \times 10^{-3}$ V A^{-2} at 1.5 T, in agreement with this explanation.
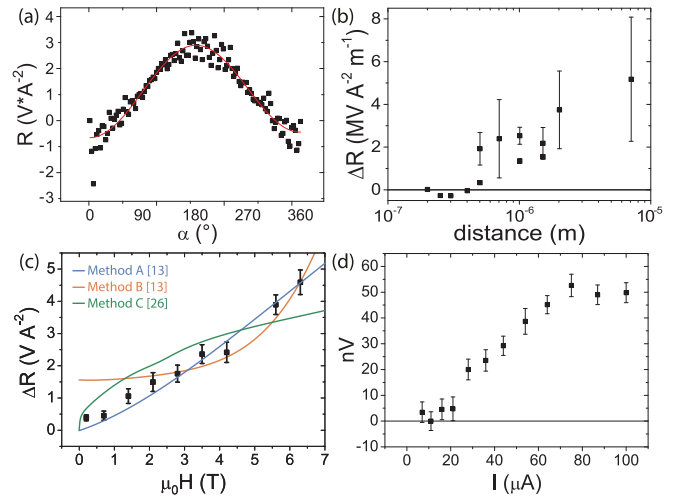

FIG. 3. The nonlocally obtained SSE signals. (a) The angle-dependent resistance at 5 K and 6.3 T. The background resistance is small in comparison to the local background resistance. (b) The second harmonic has a negative sign at distances smaller than 500 nm, similar to in thin ferromagnetic films, but after the sign change the signal increases monotonously with distance. The size of the error bars increase with distance and have a large variation between devices. (c) The signal size increases in a comparable fashion with increasing magnetic field strength as the local signal. (d) The SSE does not increase quadratically as a function of the current. Instead, the signal shows some current threshold behavior until 25 μA and increases with field until it is saturated around 75 μA.

The temperature gradient is calculated using its relation with the signal size given by [29]

$$V_{\text{SSE}} = R_N l \lambda_N \frac{2e}{\hbar} \theta_{SH} \tanh \left(\frac{t_N}{2\lambda_N} \right) S_S^z \nabla_z T, \quad (4)$$

where $R_N = 5.17$ kΩ, $l = 20 \mu$m, $t_N = 8$ nm, $\lambda_N = 1.1$ nm, and $\theta_{SH} = 0.08$ are the Pt bar resistance, the length, the thickness, the spin diffusion length, and the spin Hall angle, respectively [30]. Further, it is assumed that the NiO thickness $\gg$ the relaxation length. The temperature gradient along $\hat{z}$ near the injector with a current of 100 μA is calculated to be 2.50×10^6 K m^{-1} for method C, method A gives 7.51×10^5 K cm^{-1}, and method B results in 2.30×10^3 K cm^{-1}. This is lower compared to the calculated average temperature gradient resulting from a similar geometry on YIG at 300 K of 1.6×10^8 K cm^{-1} [13], which indicates an overestimation of the calculated S_S^z value. On the other hand, the thermal conductivity can be different in NiO at 5 K as compared to that in YIG at 300 K.

Figure 3(a) shows the angular dependence of a SSE signal obtained nonlocally at the detector and is similar to that of devices on thick YIG with a strip distance in the same range [13]. The distance dependence of the signal, shown in Fig. 3(b), shows a sign change around $d \approx 500$ nm, indicating that μ_m turns positive. Moreover, after the sign change, the signal seems to increase with increasing distance. In a YIG thin film on a GGG substrate, such sign changes are subscribed to boundary conditions at the interface of the thin film and the paramagnetic substrate. The interface will conduct little magnons while the heat is transported into GGG. Therefore,

the magnons accumulate and are reflected causing μ_m to turn positive at a certain distance from the injector and μ_m goes to zero at large distances [13]. With further increasing distances the signal in FMs drops according to a diffusion-relaxation model [2]. However, single-domain bulk FMs lack these boundaries and no positive μ_m is observed [8]. Recently, it is shown that the rotation of the pseudospin by a magnetic field could result in a sign change in the case of the presence of a Dzyaloshinskii-Moriya interaction (DMI) [31], which is not expected in NiO. The lack of a DMI also precludes the domain wall from acting as a polarizer or a retarder as described by Lan *et al.* [32], which thus cannot be a reason for a negative SSE sign in NiO. It is not fully understood why this bulk NiO shows both a sign change and the following increase in signal strength with distance. The difference between FMs and easy-axis AFMs, however, is that in AFMs there are domains present at the relevant field strengths. The partial reflection and/or absorption of magnons at domain walls could give a similar upturn of μ_m as the boundary conditions at the FM|PM interface. While S_S is altered by the magnetic field strength, this could affect μ_m such that the region where the sign change occurs is stretched. The possibility exists that the maximum reached after the sign change is then shifted towards further distances such that the signal is increasing with distance in the investigated length scale. In addition to providing an explanation for the increase in μ_m, the magnon accumulation at domain walls can be responsible for the large fluctuations between data points which increase with increasing distance due to movement of domain walls creating local variation in μ_m.

Figure 3(c) shows the magnetic field strength dependence, fitted with the same models as are used for the local data, assuming that the S_S is dominant for the change in signal strength. Also for the nonlocal signals the approach described in Ref. [16] using the dispersion from Ref. [15] best resembles the near-linear field dependence without offset. The SSE signal is driven by Joule heating and therefore expected to have a quadratic dependence on the current sent through the injector. However, after an initial increase in the current dependence, a saturation sets in around 75 μA as shown in Fig. 3(d). A strictly quadratic dependence is only expected when the parameters of the system do not change. Rising temperatures due to the current could lower the strongly temperature-dependent signal strength, leading to the saturation. The temperature increase could lower the spin Seebeck coefficient of the dependence of the magnon mode energies and their splitting by the magnetic field strength. Furthermore, an increased heat conductivity at the elevated temperature will create a lower

temperature gradient with the same heating power. Both the field dependence and the absence of an electrically injected signal resembles the results reported for Cr_2O_3 by Yuan *et al.* [5]. However, they claim this spin transport is a result of spin superfluidity.

The SSE originates from the influence of a magnetic field on the population of the magnon modes, but these models might be influenced by the movement of domain walls. The lacking offset in method B could be explained by the multidomain nature as the domains have opposite magnon spin polarization resulting in a smaller net SSE. Moreover, domain walls can interact with the spin current itself, leading to domain wall movement [33] and spin current reflection upon domain walls [34]. In thin films with multiple domain walls, the reflection damps the nonlocal signals, but domain optimization by tuning the growth direction or by magnetic training still leads to micrometer spin transport [35].

V. CONCLUSION

To conclude, we observed a spin Seebeck effect generated spin current in the bulk easy-plane antiferromagnet NiO. This was achieved as a result of an applied magnetic field without the need of exchange interactions to align the magnetic domains. The field dependence of the SSE amplitude at 5 K was modeled by the energy splitting of magnon modes, creating an imbalance in the magnon spin population. The cubic anisotropy and magnetic dipole-dipole interactions have to be taken into account in order to recreate the near-linear SSE dependence on the field and the small offset. Furthermore, the SSE signal exhibits both a sign change and then an increase with increasing the injector distance that would not be possible without the introduction of additional boundary conditions in the bulk NiO, a role that may have been fulfilled by domain walls.

[1] A. V. Chumak, V. I. Vasyuchka, A. A. Serga, and B. Hillebrands, Nat. Phys. **11**, 453 (2015).

[2] L. J. Cornelissen, J. Liu, R. A. Duine, J. B. Youssef, and B. J. Van Wees, Nat. Phys. **11**, 1022 (2015).

[3] R. Lebrun, A. Ross, S. A. Bender, A. Qaiumzadeh, L. Baldrati, J. Cramer, A. Brataas, R. A. Duine, and M. Kläui, Nature (London) **561**, 222 (2018).

[4] W. Xing, L. Qiu, X. Wang, Y. Yao, Y. Ma, R. Cai, S. Jia, X. C. Xie, and W. Han, Phys. Rev. X **9**, 011026 (2019).

[5] W. Yuan, Q. Zhu, T. Su, Y. Yao, W. Xing, Y. Chen, Y. Ma, X. Lin, J. Shi, R. Shindou, X. C. Xie, and W. Han, Sci. Adv. **4**, eaat1098 (2018).

[6] A. Qaiumzadeh, H. Skarsvåg, C. Holmqvist, and A. Brataas, Phys. Rev. Lett. **118**, 137201 (2017).

[7] L. J. Cornelissen and B. J. van Wees, Phys. Rev. B **93**, 020403(R) (2016).

[8] K. Shen, Phys. Rev. B **100**, 094423 (2019).

[9] B. Flebus, Phys. Rev. B **100**, 064410 (2019).

[10] S. M. Rezende, R. L. Rodríguez-Suárez, and A. Azevedo, Phys. Rev. B **93**, 014425 (2016).

[11] S. M. Wu, W. Zhang, A. KC, P. Borisov, J. E. Pearson, J. S. Jiang, D. Lederman, A. Hoffmann, and A. Bhattacharya, Phys. Rev. Lett. **116**, 097204 (2016).

[12] R. E. Troncoso, S. A. Bender, A. Brataas, and R. A. Duine, Phys. Rev. B **101**, 054404 (2020).

[13] J. Shan, L. J. Cornelissen, N. Vlietstra, J. Ben Youssef, T. Kuschel, R. A. Duine, and B. J. van Wees, Phys. Rev. B **94**, 174437 (2016).

[14] J. Holanda, D. S. Maior, O. Alves Santos, L. H. Vilela-Leão, J. B. Mendes, A. Azevedo, R. L. Rodríguez-Suárez, and S. M. Rezende, Appl. Phys. Lett. **111**, 172405 (2017).

[15] J. Milano and M. Grimsditch, Phys. Rev. B **81**, 094415 (2010).

[16] S. M. Rezende, A. Azevedo, and R. L. Rodríguez-Suárez, J. Appl. Phys. **126**, 151101 (2019).

[17] M. T. Hutchings and E. J. Samuelsen, Phys. Rev. B **6**, 3447 (1972).

[18] T. Kampfrath, A. Sell, G. Klatt, A. Pashkin, S. Mährlein, T. Dekorsy, M. Wolf, M. Fiebig, A. Leitenstorfer, and R. Huber, Nat. Photonics **5**, 31 (2011).

[19] M. Grimsditch, L. E. McNeil, and D. J. Lockwood, Phys. Rev. B **58**, 14462 (1998).

[20] P. R. T. Ribeiro, F. L. A. Machado, M. Gamino, A. Azevedo, and S. M. Rezende, Phys. Rev. B **99**, 094432 (2019).

[21] N. Vlietstra, J. Shan, B. J. van Wees, M. Isasa, F. Casanova, and J. Ben Youssef, Phys. Rev. B **90**, 174436 (2014).

[22] G. R. Hoogeboom, A. Aqeel, T. Kuschel, T. T. Palstra, and B. J. Van Wees, Appl. Phys. Lett. **111**, 052409 (2017).

[23] Y. T. Chen, S. Takahashi, H. Nakayama, M. Althammer, S. T. B. Goennenwein, E. Saitoh, and G. E. W. Bauer, Phys. Rev. B **87**, 144411 (2013).

[24] J. Milano, L. B. Steren, and M. Grimsditch, Phys. Rev. Lett. **93**, 077601 (2004).

[25] W. L. Roth, J. Appl. Phys. **31**, 2000 (1960).

[26] J. Fischer, O. Gomonay, R. Schlitz, K. Ganzhorn, N. Vlietstra, M. Althammer, H. Huebl, M. Opel, R. Gross, S. T. B. Goennenwein, and S. Geprägs, Phys. Rev. B **97**, 014417 (2018).

[27] I. Sänger, V. V. Pavlov, M. Bayer, and M. Fiebig, Phys. Rev. B **74**, 144401 (2006).

[28] S. M. Rezende, A. Azevedo, and R. L. Rodriguez-Suárez, J. Phys. D **51**, 174004 (2018).

[29] J. Holanda, O. Alves Santos, R. O. Cunha, J. B. S. Mendes, R. L. Rodriguez-Suarez, A. Azevedo, and S. M. Rezende, Phys. Rev. B **95**, 214421 (2017).

[30] N. Vlietstra, J. Shan, V. Castel, J. Ben Youssef, G. E. W. Bauer, and B. J. van Wees, Appl. Phys. Lett. **103**, 032401 (2013).

[31] T. Wimmer, A. Kamra, J. Gückelhorn, M. Opel, S. Geprägs, R. Gross, H. Huebl, and M. Althammer, arXiv:2008.00440.

[32] J. Lan, W. Yu, and J. Xiao, Nat. Commun. **8**, 178 (2017).

[33] R. Wieser, E. Y. Vedmedenko, and R. Wiesendanger, Phys. Rev. Lett. **106**, 067204 (2011).

[34] E. G. Tveten, A. Qaiumzadeh, O. A. Tretiakov, and A. Brataas, Phys. Rev. Lett. **110**, 127208 (2013).

[35] A. Ross, R. Lebrun, O. Gomonay, D. A. Grave, A. Kay, L. Baldrati, S. Becker, A. Qaiumzadeh, C. Ulloa, G. Jakob, F. Kronast, J. Sinova, R. Duine, A. Brataas, A. Rothschild, and M. Kläui, Nano Lett. **20**, 306 (2020).